Journal of
Materials Chemistry B

Accepted Manuscript

This article can be cited before page numbers have been issued, to do this please use: Q. Liu, T. Yang, Y. Ye, P. Chen, X. Ren, A. Rao, Y. Wan, B. Wang and Z. Luo, *J. Mater. Chem. B*, 2019, DOI: 10.1039/C8TB03233E.

ROYAL SOCIETY OF CHEMISTRY

rsc.li/materials-b

View Article Online
DOI: 10.1039/C8TB03233E

Journal Name

ARTICLE

A highly sensitive label-free electrochemical immunosensing platform based on aligned GaN nanowires array/polydopamine heterointerface modified with gold nanoparticles

Received 00th January 20xx,
Accepted 00th January 20xx

DOI: 10.1039/x0xx00000x

www.rsc.org/

Qingyun Liu,[a] Taotao Yang,[a] Yongqin Ye,[b] Ping Chen,[a] Xiaoning Ren,[a] Ai Rao,[a] Ying Wan,[a] Bin Wang*[b] and Zhiqiang Luo*[a]

Aligned GaN nanowires array shows great potential not only in optoelectronic devices, but also in sensitive biosensor applications, owing to their excellent chemical stability and biocompatibility, as well as high electron mobility and surface-to-volume ratio. However, to construct electrochemical immunosensors, proper surface modification of GaN nanowires, which can enable efficient charge transfer and provide large densities of immobilization sites for antibodies to anchor, is still challenging. Herein we demonstrate a highly sensitive label-free electrochemical immunosensing platform based on integration of polydopamine (PDA) surface chemistry on GaN nanowires surface. PDA polymer was self-assembled on GaN nanowire surfaces via organic polymerization. Interface dipole layer generated at the GaN nanowires array/PDA polymer heterointerface enabled efficient charge transfer. The aligned GaN nanowires array/PDA hybrids were further modified with gold nanoparticles for subsequent covalent binding of antibodies. The fabricated immunosensor yielded a wide linear range between 0.01 to 100 ng/ml and a detection limit as low as 0.003 ng/ml for the detection of alpha-fetoprotein (AFP). The immunosensor showed good selectivity, reproducibility, stability and was utilized in human serum samples for AFP detection. This work demonstrates the superiority of taking advantage of nanowire array configuration and semiconductor/polymer heterointerface in immunosensing platform for sensitivity enhancement.

1. Introduction

Encouraged by the unprecedented progress made in nanoscience and nanotechnology in recent years, nanostructured transducing electrodes have been developed and extensively adopted not only in optoelectronic devices, but also to assist sensitive and accurate electrochemical immunoassay.[1-7] As a controlled and systematic assembled 1D nanomaterials, nanowires array architecture with high alignment exhibits unique advantages of high surface-to-volume ratio and separate electron transfer paths. These aspects generate considerable advantages to use nanowires array as sensitive electrochemical immunosensor, since the biological interactions occurring at the transducing electrode play important role in establishing an efficient electrochemical immunosensor.[8] For example, nanowires array can provide more immobilization sites for targeted antibodies, and the specific immobilizations of antibodies on the transducing electrode surfaces improve the capture ability of biomarkers via antibody-antigen recognition, therefore facilitate the transduction of immunoreaction into electrical signals.[8] Therefore, engineered nanoarray structures have been considered as competitive nanostructured electrode candidates in constructing sensitive nanoscale immunosensors. Direct and wide bandgap gallium nitride (GaN), a well-establishing industrial optoelectronics material, is emerging recently as one of the advanced semiconductor biosensor candidates for their chemical stability, low toxicity to living cells and high electron mobility.[9-14] Most of the reports on GaN electrodes are limited to thin film configuration; for example, GaN based planar field effect transistors (FET) have been adopted in detecting DNA probe, pH changing, hydrogen gas and proteins related with cancerous diseases.[14-17] Recently, geometry- and position- controlled GaN nanowires array has commenced to receive significant attention in biosensing utilization, owing to the advantages of nanowire arrays configuration coupled with their excellent chemical stability and biocompatibility.[18-20] For example, Choi et al. reported a highly sensitive assay for cancer antigen CA15-3 detection

[a] College of Life Science and Technology, Huazhong University of Science and Technology, Wuhan 430074, China.
E-mail: zhiqiangluo@hust.edu.cn
[b] Department of General Surgery, Shenzhen Children's Hospital, Shenzhen 518026, China.
E-mail: szwb1967@126.com

†Electronic Supplementary Information (ESI) available: SEM and TEM characterization of Au NPs, HRTEM characterization of GaN nanowire/PDA/Au NPs, ideal schematic diagram of the structural and electronic properties at the GaN/PDA heterointerface, UPS and UV-vis DRS spectra of GaN, PDA and GaN/PDA, the relationship of current increment with PDA polymerization time and Au deposition time, comparisons between morphologies and resistance of GaN electrodes, detection condition optimizations, the selectivity, stability, repeatability and recovery in diluted human serum of the immunosensor. See DOI: 10.1039/x0xx00000x

employing (3-aminopropyl) triethoxy silane functionalized GaN nanowires as sensing platforms, which allow for detection of an individual fluorescence under relatively low background signal.[18] Additionally, our previous studies also demonstrate the feasibility of bare and functionalized GaN nanowires in silver ions detection.[20]

Since nanomaterials have charge carriers limited or close to the electrode/electrolyte interface, the presence of antibody-antigen complex may significantly affect the accumulation or depletion of interfacial charge carriers, thus generating remarkable readout signal change.[21] The sensitivity of GaN nanowires would be further strengthened by modulating electrode surface with proper tether organic molecules. Inspired by mussel-adhesion phenomenon, biofunctionalized GaN nanowires array would be manufactured gently through direct encapsulation using polydopamine (PDA). Actually, surface modifications of nanomaterials with PDA have enjoyed increasing interests.[22-24] The as-formed adherent PDA coating has a surface occupied with abundant active catechol and amine groups, capable to serve as reductants, binding reagents and universal platforms for secondary reactions.[22] However, in most of the cases, the build-up of the sensing electrodes are confined to couple PDA with metals (Au) or narrow bandgap semiconductors (carbon nanotubes). For example, PDA modified Au nanotubes were reported to be utilized as sensitive alpha-fetoprotein (AFP) electrochemical immunosensor.[25] Similar result was also reported on PDA coated carbon nanotubes-prussian blue modified glassy carbon electrode.[26] Semiconductors with wide bandgap have the potential to make a good match with the typical HOMO-LUMO gaps of PDA biomolecules.[19, 27] Therefore, it is expected that integration of PDA on GaN nanowires surface will enhance electrode conductivity by taking full advantages of the semiconductor/organic heterointerface.

Herein, a versatile protocol to utilize GaN nanowires array/PDA heterointerface as the sensitive transducing matrix for electrochemical immunosensor had been demonstrated. The strategy employed here was based on the combined advantages contributed from both vertically-grown GaN nanowires and functionalization with PDA polymer. The PDA-modified GaN nanowires array was further treated with gold nanoparticles (Au NPs) to obtain an increasing antibody (Ab1) immobilization amount. As a demonstration of the capability of our protocol, AFP was chosen as a model biomarker for our electrochemical immunosensor. AFP, an oncogenic glycoprotein, is one of the most extensively used cancer biomarkers.[28] Accurate early of detection AFP is of great importance in proper prevention, diagnosis and treatment of cancers, since an increasing level of AFP in human body are related to tumor cell growth and thus demonstrated to be clinical indications for several cancerous diseases such as hepatocellular, yolk sac and testicular cancer.[29] Various immunoassay methods have been reported for AFP detection, including chemiluminescence,[30] fluorescence,[31] and surface plasmon resonance.[32] For instance, Zhang's group has constructed an ultrasensitive photoelectrochemical biosensor by coupling high conductive graphite flake, graphene oxide and an alkylated C_{60} into a metal-free all-carbon nanohybrid to achieve ultralow AFP detection limit.[33] Electrochemical bioassay for AFP detection has also obtained great research interests by showing high sensitivity, low cost, ease of portability and simply instrumentation.[34-37] Using our as-developed electrochemical immunosensor based on GaN nanowires array/PDA heterointerface modified with Au NPs, the label-free detection of AFP was obtained in a wide linear range of 0.01-100 ng/ml and a detection limit as low as 0.003 ng/ml. The presented work demonstrated the feasibility of GaN nanoarray structures in the application of biological immunosensing.

2. Experimental

2.1 Reagents and materials.

P-type GaN substrates were purchased from Nanowingen Nanotechnology Company (Suzhou,China). Dopamine hydrochloride, (3-aminopropyl) triethoxy silane (APTES) and chloroauric acid ($HAuCl_4 \bullet 3H_2O$) were purchased from Sigma-Aldrich (USA). Gallium oxide (Ga_2O_3), sodium citrate, potassium ferricyanide($K_3Fe(CN)_6$) and potassium ferrocyanide($K_4Fe(CN)_6 \bullet 3H_2O$) were purchased from Sinopharm Chemical Reagent Co.,Ltd.(Shanghai, China). Alpha-fetoprotein antigen (AFP), alpha-fetoprotein monoclonal antibody (anti-AFP) and carcinoembryonic antigen (CEA) were purchased from Biocell Biotechnology Co., Ltd. (Zhengzhou, China). Bovine serum albumin (BSA), prostate specific antigens (PSA), cancer antigen 125 (CA 125), human immunoglobulin G (HIgG) were purchased from Bosaitu biotechnology company (Zhengzhou, China). Human serum purchased from Hongquan bio-tel (Guangzhou,China) were diluted by deionized water (1:99) before utilization. Phosphate buffer saline (PBS, pH=7.4) were prepared by mixing 0.1M sodium dihydrogen phosphate ($NaH_2PO_4 \bullet 2H_2O$) and 0.1M disodium hydrogen phosphate ($Na_2HPO_4 \bullet 12H_2O$) (v:v=81:19) stock solutions. All other reagents were of analytical grade and used without further purification. Ultrapure water from Milli-Q system (Millipore Direct-Q 5UV) with a resistivity of 18.2 Ω·cm were used in all experimental runs.

2.2 Apparatus.

The synthesis of GaN nanowires array was conducted in a homemade tubular furnace. The morphology and composition purity were characterized by a field-emission scanning electron microscopy operating at 20 kV (FESEM, HITACHI, SU8000) attached with a Dektak XT stylus profiler. The structure was characterized by X-ray diffraction patterns (XRD, SmartLab-SE) with Cu Kα radiation, operating at 40 kV and 40 mA. The morphology and composition distribution of individual nanowires were observed using a transmission electron microscopy operating at 200 kV (TEM, FEI, Tecnai G^2 F20) attached with an X-ray energy dispersive spectrometer (EDS). Adsorption spectra were measured on UV-vis-NIR diffuse reflectance spectroscopy (DRS, Shimadzu Corporation UV-3600) for band gap calculations. The energy levels were measured on an ultraviolet photoelectron spectroscopy (UPS, Thermo

ESCALAB 250XI) by using He I source (21.22 eV). Electrochemical measurements were carried out on Chenhua CHI660E electrochemical workstation (Shanghai, China).

2.3 Synthesis of GaN nanowires array.

GaN nanowires array were prepared through a simple chemical vapor deposition (CVD) process, as described in our previous work.[38] Briefly, α-Al_2O_3 substrate coated with a 4.5 μm GaN layer by hydrogen vapor phase deposition (HVPE) was commercially produced. Before growth, 5 nm gold layer were deposited on GaN substrates as catalyst. An alumina boat filled with Ga_2O_3 powder was placed in the center of a quartz tube in a tubular furnace. The temperature was increased to 1100 °C from room temperature under high purity gaseous ammonia protection (NH_3, 10 sccm) and kept for 30 min. After reaction, the furnace was cooled down to room temperature under protection of gaseous argon (Ar, 100 sccm). Similarly, randomly-assembled GaN nanowires (referring to GaN nanowires thereinafter) were prepared under identical condition, except to tune NH_3 flowing rate from 10 sccm to 100 sccm.

2.4 Preparation of GaN-based electrodes.

GaN nanowires were immersed in 20 ml Piranha solution (H_2SO_4:H_2O_2=3:1 v/v) and hydrochloric acid (HCl:H_2O= 1:1 v/v) for 20 min, respectively, for surface hydroxylation as well as cleaning. The samples were further coated with polydopamine (PDA) via a simple dip-coating method.[22] First, 0.06057 g Tri(hydroxymethyl)aminomethane (Tris) was dissolved in 25 ml deionised water to obtain 20 mM Tris solution. The pH of the Tris solution was adjusted by 20mM HCl solution to reach pH=8.5 and then diluted with deionised water to make 50 ml. Second, the as-synthesized GaN nanowires array samples were dipped and suspended in 50 ml 10mM Tris-HCl (pH=8.5). The samples were kept vertical to prevent non-specific microparticle deposition. Thrid, 0.01 g dopamine hydrochloride were added into the Tris-HCl buffer solution under gentle stirring for certain hours. The mixture solution turned to dark brown and finally dark grey during pH-induced oxidation reaction. The samples coated with PDA were gently rinsed with deionized water several times and dried with N_2 gas. The as-obtained samples were stored at 4 °C for later use.

2.5 Synthesis of Au NPs-decorated PDA-coated GaN nanowires array.

At first, uniform gold colloids with ca.13 nm in diameter were prepared by rapid injecting 5 ml 38.8nM sodium citrate into 50 ml 1mM $HAuCl_4$ boiling solution under vigorous stirring.[39] After boiling for 15 min, the solution was cooled down to room temperature and stored at 4 °C for later use. The as-obtained dark red solution was characterized and presented in Figure S1. The PDA-coated GaN nanowires array samples were immersed in 3 ml gold colloidal solution and placed in a constant temperature oscillator (37 °C, 200R) overnight. Later, the samples were rinsed with deionized water and dried by N_2 gas. GaN thin film/PDA/Au NPs and GaN nanowires/PDA/Au NPs were prepared through identical procedure. GaN nanowires array decorated with Au NPs was treated with a slight difference. GaN nanowires were first treated in Piranha solution at 80°C for 50 min. After rinsing with denoised water, they were immersed in 1% (v/v) 3-APTES in ethanol at room temperature for 1h under constant shaking (25 °C, 100R). Then they were rinsed with ethanol and placed on a hot plate at 120°C for 10 min, respectively. Au NPs deposition process was the same with above-mentioned.

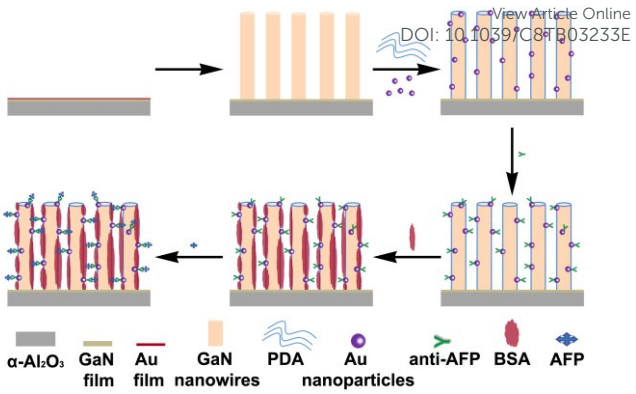

Scheme 1 General strategy for the fabrication process of GaN nanowires array/PDA/Au NPs immunosensor.

2.6 Construction of the immunosensor.

The general strategy for the immunosensor construction was displayed in Scheme 1. Firstly, the GaN nanowires array/PDA/Au NPs electrodes were immersed in 9.323 ug/ml

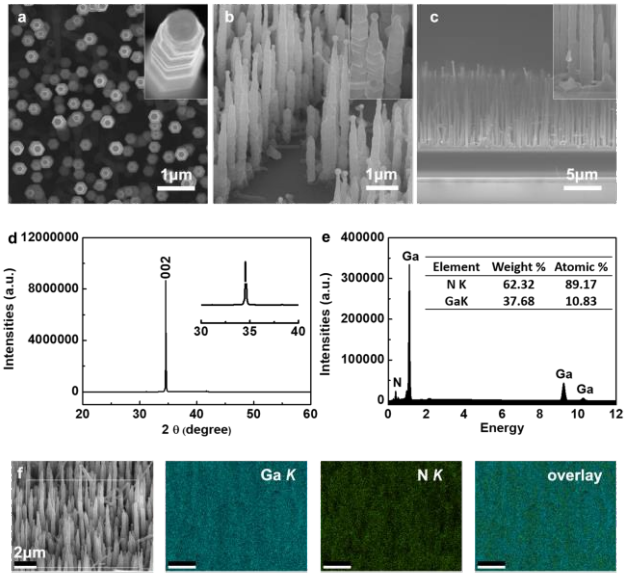

Figure 1 (a-c) Low magnification plan view, 40°-tilted and cross-sectional SEM images for highly-aligned GaN nanowires array (from left to right), a GaN layer with 4.5 μm thickness can be observed from (c); Insets show the magnified SEM images for an individual nanowire. (d) XRD pattern of highly-aligned GaN nanowires array, a predominant peak is observed at 34.55°, indexed as (002) plane in wurtzite GaN crystal; Inset in (d) emphasized the diffraction peak at 34.55°. (e) EDS spectrum shows distinctive Ga and N peaks and (f) the corresponding EDS elemental mapping shows exclusive Ga and N elements. In (f) from left to right represents SEM, Ga K, N K, and overlay image, respectively.

anti-AFP antibody solution and incubated at 37 °C. Then they were gently washed with 0.1M PBS (pH=7.4) to exclude any physically adsorbed antibodies. Secondly, to avoid non-specific adsorption, the modified electrodes were immersed in 1 mg/ml BSA solution for extra sites blocking and rinsed with PBS. Lastly, the modified electrodes were immersed in AFP antigen solution of a specific concentration and incubated at 37 °C. After gentle washing in PBS, the immunosensors used for electrochemical characterization were obtained.

2.7 Electrochemical characterization.

All electrochemical measurements were carried out on an electrochemical workstation at room temperature. A standard three-electrode configuration was adopted for the electrolytic system, including GaN as working electrode, a platinum tablet (5 mm × 5 mm) as counter electrode and Ag/AgCl (3 M KCl) as reference electrode. The working electrodes were fixed with an electrode holder and immersed in a electrolyte solution containing 5 mM $K_3Fe(CN)_6/K_4Fe(CN)_6$ (1:1) and 0.1 M KCl, where $[Fe(CN)_6]^{4-/3-}$ acted as redox probes. Cyclic voltammetry (CV) and electrochemical impedance spectra (EIS) were adopted in each electrode modificati-on and immunosensor fabrication process. Differential pulse voltammetry (DPV) were adopted in calibration process. CV spectra were recorded at applied potential from -0.6 V to 1.0 V (vs Ag/AgCl) at a scan rate of 100 mV/s. EIS were recorded in frequency ranges of 0.1 Hz to 10000 Hz, with amplitude of 5 mV. DPV were captured at applied potential from -0.2 V to 0.6 V (vs Ag/AgCl).

3. Results and discussion

3.1 Characterization of GaN nanowires array polydopamine/gold nanoparticles composite.

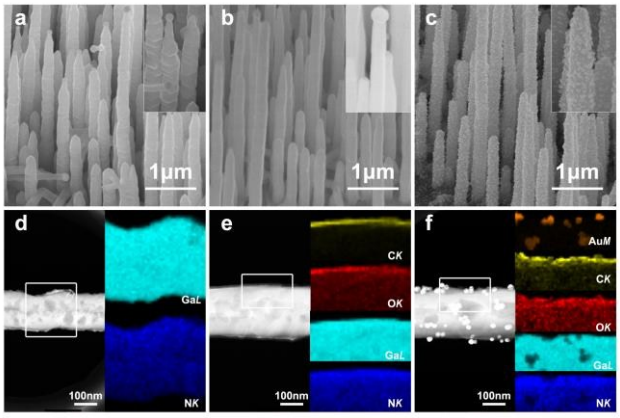

Figure 2 Representative 40°-tilted SEM images for (a) GaN nanowires array, (b) GaN nanowires array/PDA and (c) GaN nanowires array/PDA/Au NPs; insets display the morphology of individual nanowire after each assembly step. STEM images for an individual nanowire after each step and its corresponding spatially resolved elemental mappings are shown in (d-f), respectively. The selected areas for compositional analysis are pointed out by white circles at left side.

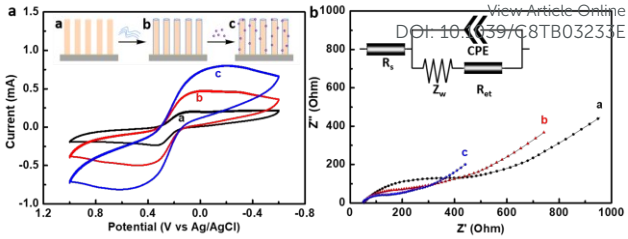

Figure 3 (a) Variation of cyclic voltammograms and (b) electrochemical impedance spectra with the modified GaN nanowires array at a scan rate of 100 mV/s: a. bare GaN nanowires array, b. GaN nanowires array/ PDA, c. GaN nanowires array/PDA/Au NPs; A corresponding schematic diagram are presented at top in (a) to describe the modification process; An electronic equivalent circuit presented at top in (b) is used to model interfacial phenomenon, where R_s represents ohmic resistance of $[Fe(CN)_6]^{3-/4-}$ electrolyte, Z_w represents Warburg impedance, R_{et} is electron transfer resistance and CPE represents capacitance of GaN nanowires array electrode with rough surface.

Figure 1a-c presented plan view, 40°-tilted and cross-sectional scanning electron microscopy (SEM) images of GaN nanowires array prepared by a simple CVD method. A large scale of nanowires was observed to grown on heavily-doped p-type GaN substrate with uniform alignment. From low magnification SEM image in Figure 1c, it can be seen that highly-aligned GaN nanowires were epitaxially grown on GaN buffer layer (with thickness of ca. 4.5 μm). The inserted magnified SEM images revealed that GaN nanowires were ca. 200 nm in diameter, up to 10 μm in length, featured with hexagonal cross section with catalytic gold nanoparticles (Au NPs) on the tips. Contrary to commonly observed smooth side facets, the vertically-aligned GaN nanowires exhibited periodic corrugated morphology, as indicated in inset in Figure 1a-b. It is assumed that the periodic concave and convex crystalline planes are contributed by the oscillation in nanowires' radial growth, combined with electrostatic interaction energy equilibrium.[38] Structural analysis with XRD proved the vertically-grown nanowires to be wurtzite GaN single crystal with high alignment along [001], by showing a predominant and singular diffraction peak at 34.55° indexed as (002) planes (Figure 1d). Quantitative composition analysis on the GaN nanowires also confirmed high purity of the GaN nanowires by showing exclusive N and Ga elements (Figure 1e). Elemental mapping of a randomly selected area revealed uniform distribution of Ga and N elements (Figure 1f).

GaN nanowires array was dipped in Tric-HCl buffer solution dissolving 0.01g dopamine hydrochloride for polydopamine (PDA) coating. After coating with PDA, the substrate slice displayed light grey in color, while substrate with bare GaN nanowires usually displayed light yellow. Then it was immersed in nanogold colloidal solution to allow for gold nanoparticles (Au NPs) absorption onto the nanowire surfaces. At this time, the substrate turned to dark red, indicating the successful deposition of Au NPs. Figure 2a-c presented

representative SEM images for GaN nanowires array in stepwise modification processes. After PDA coating, the nanowire surfaces became smoother (Figure 2b) compared with that of bare GaN nanowires, where the latter was featured with periodic corrugated side facets (Figure 2a). In Figure 2c, Au NPs were observed to distribute uniformly on the surfaces of GaN nanowires array/PDA hybrid.

Scanning transmission electron microscopy (STEM) was adopted to observe the morphology and characterize the compositional distribution of individual nanowires at atomic scale. Before modification, bare crystalline GaN nanowire exhibited two elements, Ga element and N element, in consistent with quantitative composition analysis performed in SEM characterization (Figure 2d). Two additional signals, C and O elements, were collected from GaN nanowire coated with PDA, provided another evidence for the existence of PDA (Figure 2e). It is worthy to notice that both C and O signal were strong at top but became weaker along radial direction. This is possibly due to the comparative stronger Ga and N signals originated from GaN nanowires. Similarly, GaN nanowire/PDA hybrid/Au NPs exhibited distinctive Au signals apart from Ga, N, C and O signals (Figure 2f). Consistent results can also be observed in transmission electron microscopy (TEM) images (Figure S2a-c). High-resolution TEM in Figure S2d revealed succinct diffraction spots of single crystallien Au NP and GaN nanowire, as well as PDA coating on the nanowire surface.

3.2 Optimization of the modified GaN nanowires array.

The electrochemical performance of the stepwise modified GaN nanowires array were monitored by cyclic voltammograms (CV) and electrochemical impedance spectroscopy (EIS) measurements. Figure 3 displayed the CV and EIS curves of the modified GaN nanowires array electrodes characterized in 0.5 mM $[Fe(CN)_6]^{3-/4-}$ and 0.1M KCl electrolyte after each assembling step. In Figure 3a, CV plot of bare GaN nanowires array showed significant oxidation and reduction peaks at scanning rate of 100 mV/s in the range from -0.6 V (vs Ag/AgCl) to 1 V (vs Ag/AgCl), suggesting highly reversible electrochemical reactions at electrode surface. Coating of PDA layer on the GaN nanowiresnmade the peak current increase over the voltage range, indicating the charge transfer between GaN nanowires and PDA linker was promoted. Thereafter, Au NPs deposition gave a further increase in current signal, which could be attributed to the good conductivity of nanogolds. Subsequently, impedance measurements were adopted to analyses detailed information on electrical resistance and capacitance changes at the heterointerface. EIS results were presented in Figure 3b by Niquist plots, imaginary impedance Z''(ω) vs real impedance Z'(ω), of stepwise modified GaN nanowires array electrode. The Z'(ω) and Z''(ω) are adjusted to the same scale in order to show the angle of inclined line at low frequency region.[40] The impedance spectrum included a 30° inclined line at low frequency region (diffusion limited process) and a semicircle at higher frequency region (electron transfer dominated process). As the modification process proceeded, the semicircles in higher frequency region decreased in sequence of GaN nanowires array, GaN nanowires array/PDA and GaN nanowires array/PDA/Au NPs. The semicircle diameter equals to the electron transfer resistance Ret. From the fitted parameters shown in Table S1, it can be inferred that the R_{et} values were decreased significantly from 448.2 Ω (GaN nanowires array) to 188.2 Ω (GaN nanowires array/PDA) and 96.04 Ω (GaN nanowires array/PDA/Au NPs). Thus, the smaller semicircles diameter indicated the smaller electron transfer resistance, in other words, the electron transfer step became faster at the surface of modified electrode,[41] which is consistent with results in CV measurement.

Generally, the R_{et} value of PDA is associated with polymerization time.[42] The relationship of current increment (ΔI) with PDA polymerization time was characterized by CV and summarized in Figure S3a. It can be inferred that the current

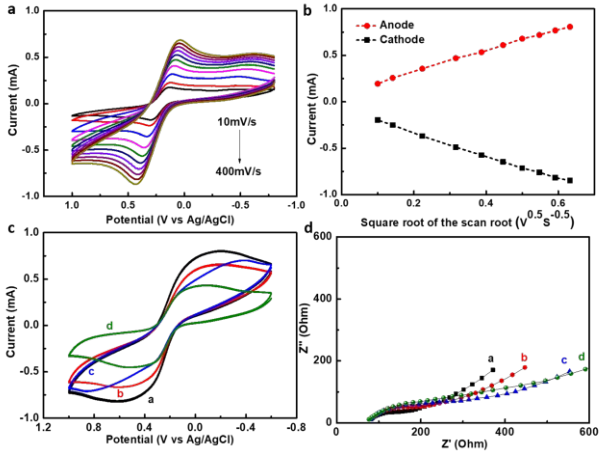

Figure 4 (a) Cyclic voltammograms of bare GaN nanowires array at different scan rate (10 mV/s, 20 mV/s, 50 mV/s, 100 mV/s, 150 mV/s, 200 mV/s, 250 mV/s, 300 mV/s, 350 mV/s, 400 mV/s); (b) Corresponding cathodic (black) and anodic (red) peak currents versus square root of scan rates from 10mV/s to 400mV/s in (c); (c) Cyclic voltammograms and (d) electrochemical impedance spectra of the electrode after each step of fabrication process: a. GaN nanowires array/PDA/Au NPs, b. GaN nanowires array/PDA/Au NPs/Ab1, c. GaN nanowires array/PDA/Au NPs/Ab1/BSA, d. GaN nanowires array/PDA/Au NPs/Ab1/BSA/AFP.

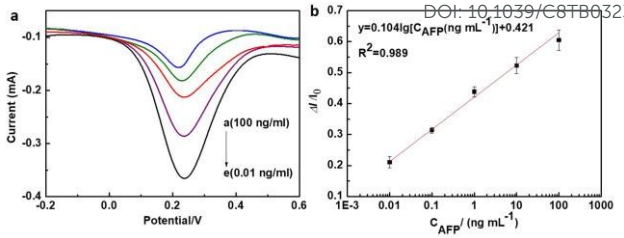

Figure 5 (a) Differential pulse voltammetry of the as-prepared immunosensors in the presence of AFP with different concentration (0.01 ng/ml, 0.1 ng/ml, 1 ng/ml, 10 ng/ml, 100 ng/ml). (b) Corresponding calibration curve for AFP detection, the error bars represent the standard deviation obtained from three measurements (n=3).

View Article Online
DOI: 10.1039/C8TB03233E

Table 1 Comparison of immunoassay performance of the proposed immunosensor with different AFP immunosensors.

Immunosensors	Linear range (ng/ml)	Detection limit (ng/ml)	References
ITO/TiO_2/ CdS	5×10^{-2}-50	4×10^{-2}	43
Ag wire-graphene	5×10^{-2}-400	5×10^{-3}	44
MWCNTs/SiO_2 nanoparticles array	10^{-1}-30	2×10^{-2}	45
PDA/ZnO nanorods	10^{-1}-500	10^{-2}	46
Au NPs/PDA/GaN nanowires array	10^{-2}-100	3×10^{-3}	This work

increased significantly with PDA polymerization time from 1h to 5h. This might be attributed to the decreased R_{et} value at the GaN/PDA heterointerface. However, the current change was not obvious when the polymerization time extending from 5h to 20h. Therefore, 5h was chosen as the optimal polymerization time. From the HRTEM images (Figure S2d) it can be estimated that the thickness of PDA layer reached 5 nm after 5h. The Au NPs densities were also investigated by dipping the electrodes in colloidal Au solution for different times. The current reached maximum after 12h deposition and remained unchanged since then. Thus, the Au NPs deposition time was chosen to be 12h (Figure S3b).

To this end, direct bandgap GaN nanowires appear to be a suitable candidate semiconductor to make electronic contact with PDA dueto its wide bandgap (3.4 eV)[38] and few defects at the interface (Figure S2d). It is believed that heterointerfaces between semiconductors and biomolecules are beneficial for electrochemistry application. In an ideal situation, biomolecules are covalently immobilized on the semiconductor surface via proper mediate, namely linker molecules. The influence of an interface dipole layer (IDP) and of interface defects are necessary to consider, as depicted in Figure S4a. In order to promote the electronic properties, defects at interface with area densities below 10^{11} to 10^{12} have to be ensured.[27] On the other hand, the potential energy jump caused by IDP can have a significant effect on the overall electronic properties. The band offset occurring at the IDP is closely related to the position of molecular electronic levels in linker molecules, i.e. the highest occupied molecular orbital (HOMO) and the lowest unoccupied molecular orbital (LUMO). From the energy levels of GaN and PDA shown in Figure 4a, which are determined by ultraviolet photoelectron spectroscopy (UPS, Figure S4b-c) and UV-vis diffuse reflectance spectroscopy (DRS, Figure S4d-f), it is suggested that efficient charge transfer between wide bandgap semiconductors and linker molecules is possible due to the relatively small electronic barriers.[47]

The morphologies of GaN electrodes were manipulated to investigate the structure-electronic properties relationship. Figure S5a-c showed SEM images for modified GaN electrodes with diverse morphologies. The corresponding Niquist plot was represented in Figure S5e. It can be clearly seen that GaN nanowires array/PDA/Au NPs electrode exhibited the smallest semicircle diameter, GaN nanowires /PDA/Au NPs the larger and GaN film/PDA/Au NPs the largest; the R_{et} value was GaN nanowires array/PDA/Au NPs< GaN nanowires/PDA/Au NPs < GaN film/PDA/Au NPs. The influence of PDA coating to R_{et} value was also investigated. The semicircle diameter of GaN nanowires array/Au NPs was larger than that of both GaN nanowires array and GaN nanowires modified with PDA and Au NPs, but smaller than GaN film/PDA/Au NPs (Figure S5e). These results illustrated that conductivity of GaN nanowires with high alignment is superior than either randomly-assembled or planar counterparts, which might be attributed to the high electron mobility of GaN nanowires assembled onto the conductivity layer while the conductive layer acted as transport channel.[20] In addition, PDA/Au NPs modified GaN nanowires exhibited better conductivity than GaN nanowires covalently functionalized with Au NPs, which might be ascribed to the GaN/PDA heterointerface.[47]

3.3 Construction of GaN nanowires array based immunosensors.

The electrochemical properties of the modified GaN nanowires array electrode were characterized before immunosensor fabrication. Figure 4a showed the relationship between scanning rates and peak currents in the modified GaN nanowires array/PDA/Au NPs electrode. Well-defined redox waves were observed at scanning rates from 10 mV/s to 400 mV/s, with ΔE_p and I_{ox}^P/I_{red}^P of 165 mV and 0.989 at scanning rate of 10 mV/s. The corresponding anodic and cathodic peak currents showed a linear dependence on the square root of scanning rate (Figure 4b). It can be deduced that the electrochemical reaction on GaN nanowires surface are mass-transfer controlled.

The step-by-step fabrication process and the electrochemical performances of the immunosensor were monitored by CV and EIS measurements. As indicated in Figure 4c, CV plot of GaN nanowires array/PDA/Au NPs exhibited two well-defined reduction and oxidation peaks. After continuous loading of Ab1, BSA and AFP on the electrode surface, the current responses decreased gradually, which were caused by inhibited interfacial electron transfer. This could be easily understood since the insulating immobilized proteins usually exhibit poor conductivity and is expected to retard the charge transfer kinetics at the electrode surface. The electrochemical impedance during the immunosensor fabrication process was also presented by Nyquist plot in Figure 4d. It can be observed that the diameters of the semicircles on the Nyquist plots increased with the successive assembly of Ab1, BSA and AFP on the electrode surface, which indicated the interfacial electron transfer resistance grew larger. The consistent results

in CV and EIS spectrum confirmed the successful construction of the GaN nanowires array/PDA/Au NPs immunosensor.

Prior to detection of AFP, the detection conditions were optimized for better analytical performance. The incubation time for anti-AFP antibody and AFP antigen are important factors, and thus have been carefully examined. Figure S6a revealed a rapid inhibition ratio increase of current response from 60 min to 120 min, but afterwards a slight change was observed from 60 min to 180 min. This could be resulted from saturated number of antibodies binding on the electrode surface after 120 min. Therefore, 120 min was chosen as incubation time for anti-AFP antibody. The influence of AFP incubation time was investigated using 1 ng/ml AFP. Figure S6b showed that the current response inhibition ratio increased with incubation time and reached to maximum after 120 min, indicating the saturated AFP antigens on anti-AFP antibodies after 120 min. Thus, 120 min was chosen as incubation time for AFP antigen.

Under optimal conditions, the sensitivity and dynamic range of the as-prepared immunosensor was evaluated by differential pulse voltammetry (DPV). The fabricated immunosensor was adopted for antigen detections with different AFP concentrations from 0.01 ng/ml to 100 ng/ml. Figure 5a showed the DPV peak currents decreased with the incremental AFP concentrations in the detecting range. The corresponding calibration plots displayed a good linear detection relationship between the peak current inhibition ratio and the examined AFP antigen concentrations with a correlation coefficient of R^2=0.989 (Figure 5b). The linear relationship was established to be

$$y = 0.421 + 0.104 \lg[C_{AFP}(ng/ml)] \quad (1)$$

and the detection limit was estimated to be 0.003 ng/ml. The analytic performance of the GaN nanowires array/PDA/Au NPs immunosensor had been compared with other semiconductor and carbon nanomaterials-based immunosensors in the detection of AFP (Table 1). As can be seen, the proposed immunosensor exhibited comparable sensitivity and lower detection limit.

The selectivity, repeatability and stability of the immunosensor are important factors in the biological application. Firstly, the selectivity was investigated by adding several potential interferences, including carcinoembryonic antigen (CEA), bovine serum albumin (BSA), prostate specific antigens (PSA), human immunoglobulin G (IgG) and cancer antigen 125 (CA 125), to the immunosensor separately (Figure S7a). The inhibition ratios of the interference biomolecules were less than 5% except for CA 125, which was also less than 8%. Compared with the inhibition ratio obtained from 0.1 ng/ml AFP antigen, the variation caused by high concentration interference substances was negligible. The stability was investigated by checking current responses periodically (Figure S7b). The immunosensor exhibited initial inhibition ratio of 43.82%. After 7 days and 15 days restoring at 4 °C, it retained 40.79% and 39.44%, respectively, which demonstrated that the immunosensor was stable. Lastly, the repeatability was examined by detecting five independent immunosensors constructing with 1 ng/ml AFP antigen under identical conditions. The relative standard deviation (RSD) was 4.98%, suggesting the stability was acceptable (Figure S7c). These results confirmed the excellent selectivity, repeatability and stability of the immunosensor for AFP detection. To evaluate practicability of the immunosensor in real sample detection, a series amount of AFP was added into diluted human serum and the detection results were displayed in Table S2. The recovery was between 98.42% and 105.70% and the RSD was below 5%, which indicated the immunosensor possessed relatively good accuracy in real sample detection. The concentration range of AFP in human serum for several common neoplasms are listed in Table S3, and it can be seen that the immunosensor is capable for practical applications.

3. Conclusions

In summary, PDA/Au NPs modified highly-aligned GaN nanowires array proved to be a competitive candidate in realizing ultrasensitive label-free electrochemical immunosensors. By taking the advantage of nanoarray geometry and IDP formed at the heterointerface of wide bandgap GaN/organic PDA dendrimer, the working electrode showed reduced electron transfer resistance by showing low detection limit down to 0.003 ng/ml. Comparative studies on the surface resistance conducted on randomly-assembled and film counterparts revealed the excellent conductivity of the GaN nanowires array/PDA/Au NPs immunosensor. Furthermore, the immunosensor yielded satisfactory selectivity, stability, reproducibility and exhibited acceptable quantitative determination of AFP in human serum samples. GaN nanowires array emerges as a potential candidate in biosensing and could be utilized as effective electrode for other biomolecule detections.

Conflicts of interest

The authors declare no no conflicts of interest.

Acknowledgements

This work was supported by the China Postdoctoral Science Foundation project (grant number 2017M622431), Zhiqiang Luo and Bin Wang acknowledge support from Sanming Project of Medicine in Shenzhen (grant number SZSM201812055).

References

1. T. Cossuet, J. Resende, L. Rapenne, O. Chaix-Pluchery, C. Jimenez, G. Renou, A. J. Pearson, R. L. Z. Hoye, D. Blanc-Pelissier, N. D. Nguyen, E. Appert, D. Munoz-Rojas, V. Consonni and J. L. Deschanvres, *Advanced Functional Materials*, 2018, 28, 12.
2. S. Lu, Q. Liao, J. Qi, S. Liu, Y. Liu, Q. Liang, G. Zhang and Y. Zhang, *Nano Res.*, 2016, 9, 372-379.
3. C. Xie, B. Nie, L. H. Zeng, F. X. Liang, M. Z. Wang, L. B. Luo, M. Feng, Y. Q. Yu, C. Y. Wu, Y. C. Wu and S. H. Yu, *Acs Nano*, 2014, 8, 4015-4022.

4. A. M. Munshi, D. L. Dheeraj, V. T. Fauske, D. C. Kim, A. T. J. van Helvoort, B. O. Fimland and H. Weman, *Nano Lett.*, 2012, 12, 4570-4576.
5. Y. B. Tang, X. H. Bo, C. S. Lee, H. T. Cong, H. M. Cheng, Z. H. Chen, W. J. Zhang, I. Bello and S. T. Lee, *Advanced Functional Materials*, 2008, 18, 3515-3522.
6. J. M. Moon, Y. H. Kim and Y. Cho, *Biosensors & Bioelectronics*, 2014, 57, 157-161.
7. G. D. Sulka, K. Hnida and A. Brzozka, *Electrochimica Acta*, 2013, 104, 536-541.
8. H. Ogi, S. Iwagami, A. Nagakubo, T. Taniguchi and T. Ono, *Sens. Actuator B-Chem.*, 2019, 278, 15-20.
9. L. E. Bain and A. Ivanisevic, *Small*, 2015, 11, 768-780.
10. M. Hofstetter, J. Howgate, M. Schmid, S. Schoell, M. Sachsenhauser, D. Adiguzel, M. Stutzmann, I. D. Sharp and S. Thalhammer, *Biochem. Biophys. Res. Commun.*, 2012, 424, 348-353.
11. C. P. Chen, A. Ganguly, C. Y. Lu, T. Y. Chen, C. C. Kuo, R. S. Chen, W. H. Tu, W. B. Fischer, K. H. Chen and L. C. Chen, *Anal. Chem.*, 2011, 83, 1938-1943.
12. T. H. Young and C. R. Chen, *Biomaterials*, 2006, 27, 3361-3367.
13. R. Kirste, N. Rohrbaugh, I. Bryan, Z. Bryan, R. Collazo and A. Ivanisevic, in *Annual Review of Analytical Chemistry, Vol 8*, eds. R. G. Cooks and J. E. Pemberton, 2015, vol. 8, pp. 149-169.
14. S. J. Pearton, B. S. Kang, S. K. Kim, F. Ren, B. P. Gila, C. R. Abernathy, J. S. Lin and S. N. G. Chu, *Journal of Physics-Condensed Matter*, 2004, 16, R961-R994.
15. B. S. Kang, S. J. Pearton, J. J. Chen, F. Ren, J. W. Johnson, R. J. Therrien, P. Rajagopal, J. C. Roberts, E. L. Piner and K. J. Linthicum, *Applied Physics Letters*, 2006, 89, 3.
16. B. S. Kang, H. T. Wang, T. P. Lele, Y. Tseng, F. Ren, S. J. Pearton, J. W. Johnson, P. Rajagopal, J. C. Roberts, E. L. Piner and K. J. Linthicum, *Applied Physics Letters*, 2007, 91.
17. I. Sarangadharan, A. Regmi, Y. W. Chen, C. P. Hsu, P. C. Chen, W. H. Chang, G. Y. Lee, J. I. Chyi, S. C. Shiesh, G. B. Lee and Y. L. Wang, *Biosensors & Bioelectronics*, 2018, 100, 282-289.
18. M. K. Choi, G. S. Kim, J. T. Jeong, J. T. Lim, W. Y. Lee, A. Umar and S. K. Lee, *Sci Rep*, 2017, 7, 12.
19. C. P. Chen, A. Ganguly, C. H. Wang, C. W. Hsu, S. Chattopadhyay, Y. K. Hsu, Y. C. Chang, K. H. Chen and L. C. Chen, *Anal. Chem.*, 2009, 81, 36-42.
20. Q. Y. Liu, B. D. Liu, F. Yuan, H. Zhuang, C. Wang, D. Shi, Y. K. Xu and X. Jiang, *Appl. Surf. Sci.*, 2015, 356, 1058-1063.
21. X. Li and X. Y. Liu, *Nanoscale*, 2017, 9, 7320-7341.
22. H. Lee, S. M. Dellatore, W. M. Miller and P. B. Messersmith, *Science*, 2007, 318, 426-430.
23. C. Liu, W. Yao, M. Tian, J. Wei, Q. Song and W. Qiao, *Biomaterials*, 2018, 179, 83-95.
24. I. H. Kim, T. Yun, J.-E. Kim, H. Yu, S. P. Sasikala, K. E. Lee, S. H. Koo, H. Hwang, H. J. Jung, J. Y. Park, H. S. Jeong and S. O. Kim, *Adv. Mater.*, 2018, 30.
25. F. Peng, M. L. Chu, J. J. Sun, Y. H. Liu, Q. C. Zhang, Y. J. Chen, F. H. Wang and W. B. Zhao, *J. Electroanal. Chem.*, 2018, 814, 52-58.
26. K. Gao, Z. Sun, B. G. Pan, X. W. Qiao and C. L. Hong, *Micro Nano Lett.*, 2018, 13, 58-62.
27. M. Stutzmann, J. A. Garrido, M. Eickhoff and M. S. Brandt, *Phys. Status Solidi A-Appl. Mat.*, 2006, 203, 3424-3437.
28. H. Ikeda, Y. Sato, N. Yoneda, K. Harada, M. Sasaki, S. Kitamura, Y. Sudo, A. Ooi and Y. Nakanuma, *Hum Pathol*, 2012, 43, 1955-1963.
29. A. Forner, R. Vilana, C. Ayuso, L. Bianchi, M. Sole, J. R. Ayuso, L. Boix, M. Sala, M. Varela, J. M. Llovet, C. Bru and J. Bruix, *Hepatology*, 2008, 47, 97-104.
30. Z. H. Chen, Y. Liu, Y. Z. Wang, X. Zhao and J. H. Li, *Anal. Chem.*, 2013, 85, 4431-4438.
31. T. Yamashita, J. Ji, A. Budhu, M. Forgues, W. Yang, H.-Y. Wang, H. Jia, Q. Ye, L.-X. Qin, E. Wauthier, L. M. Reid, H. Minato, M. Honda, S. Kaneko, Z.-Y. Tang and X. W. Wang, *Gastroenterology*, 2009, 136, 1012-1024.
32. Y. Teramura and H. Iwata, *Analytical Biochemistry*, 2007, 365, 201-207.
33. Q. Zhou, H. J. Xue, Y. Y. Zhang, Y. Q. Lv, H. G. Li, S. Q. Liu, Y. F. Shen and Y. J. Zhang, *ACS Sens.*, 2018, 3, 1385-1391.
34. Y. Zhang, D. Pan, Q. Zhou, J. Zhao, N. Pan, Y. Zhang, L.-x. Wang and Y. Shen, *Journal of Materials Chemistry B*, 2018, 6, 8180-8187.
35. Z. Wang, N. Sun, Y. He, Y. Liu and J. Li, *Anal. Chem.*, 2014, 86, 6153-6159.
36. X. Lu, Z. Wen and J. Li, *Biomaterials*, 2006, 27, 5740-5747.
37. Q. A. Zhang, Y. Qiao, F. Hao, L. Zhang, S. Y. Wu, Y. Li, J. H. Li and X. M. Song, *Chemistry-a European Journal*, 2010, 16, 8133-8139.
38. Q. Liu, B. Liu, W. Yang, B. Yang, X. Zhang, C. Labbe, X. Portier, V. An and X. Jiang, *Nanoscale*, 2017, 9, 5212-5221.
39. S. H. Liu and M. Y. Han, *Advanced Functional Materials*, 2005, 15, 961-967.
40. Y. Q. Lv, S. Y. Chen, Y. F. Shen, J. J. Ji, Q. Zhou, S. Q. Liu and Y. J. Zhang, *J. Am. Chem. Soc.*, 2018, 140, 2801-2804.
41. E. Katz and I. Willner, *Electroanalysis*, 2003, 15, 913-947.
42. F. Yu, S. G. Chen, Y. Chen, H. M. Li, L. Yang, Y. Y. Chen and Y. S. Yin, *J. Mol. Struct.*, 2010, 982, 152-161.
43. W. U. Wang, C. Chen, K. H. Lin, Y. Fang and C. M. Lieber, *Proc. Natl. Acad. Sci. U. S. A.*, 2005, 102, 3208-3212.
44. J. Tang, D. P. Tang, B. L. Su, Q. F. Li, B. Qiu and G. N. Chen, *Electrochimica Acta*, 2011, 56, 8168-8175.
45. R. P. Liang, Z. X. Wang, L. Zhang and J. D. Qiu, *Sens. Actuator B-Chem.*, 2012, 166, 569-575.
46. Y. Yang and W. H. Hu, *Talanta*, 2017, 166, 141-147.
47. P. Sahoo, S. Suresh, S. Dhara, G. Saini, S. Rangarajan and A. K. Tyagi, *Biosensors & Bioelectronics*, 2013, 44, 164-170.

View Article Online
DOI: 10.1039/C8TB03233E

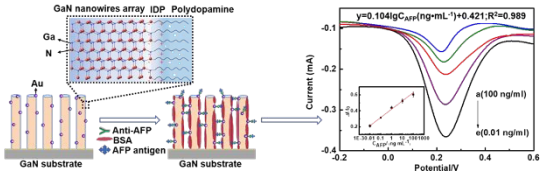

Taking advantage of nanowire array configuration and semiconductor/polymer heterointerface, a highly sensitive label-free electrochemical immunosensing platform was developed through integration of polydopamine (PDA) surface chemistry on aligned GaN nanowires surface.